Tertiary butylation of phenol over mesoporous H–FeMCM-41

Sushanta K. Badamali, Ayyamperumal Sakthivel and Parasuraman Selvam *

Department of Chemistry, Indian Institute of Technology, Powai, Mumbai 400 076, India
E-mail: selvam@ether.chem.iitb.ernet.in

Received 8 April 1999; accepted 18 January 2000

Trivalent-iron-substituted mesoporous molecular sieve catalysts (FeMCM-41) were synthesized hydrothermally and characterized systematically by various analytical and spectroscopic techniques. Temperature-programmed desorption studies of ammonia of the protonated catalyst (H–FeMCM-41) indicate a broad distribution of the acid sites. Vapour-phase alkylation of phenol with t-butyl alcohol (2-methyl-2-propanol) was carried out over this solid acid catalyst and p-t-butyl phenol was obtained as the major product with high selectivity.

Keywords: mesoporous molecular sieves, H–FeMCM-41, butylation of phenol, solid acid catalyst

1. Introduction

The p-isomers of alkyl substituted phenols are widely used in the manufacture of phenolic resins, antioxidants and polymerization inhibitors [1]. Numerous reports on the production of these alkyl-substituted phenols are available in literature [2–15], some of which are patents. Alkylation of phenol, in general, leads to thermodynamically favorable m-isomer rather than the o- and/or p-isomers. However, the presence of a phenolic group in the reactant under consideration kinetically favours the latter. Although the o-isomer is kinetically more favorable than the p-isomer, the former isomerizes easily into stable p-isomer owing to steric hindrance at the ortho position [12,13]. Further, the selectivity of the products depends mainly on the nature of the acidic sites (figure 1) present on the catalyst [7]. For example, the weakly acidic (ultrastable) zeolite-Y [8] leads to O-alkylated product (phenol alkyl ether), while the strongly acidic zeolite-β [14] results in C-alkylated product, viz., the m-isomer. This is produced by the isomerization of initially formed o- and p-alkylated products [7,11]. On the other hand, moderately acidic catalysts, like SAPO-11 [2], ZSM-12 [3], zeolite-Y [6] and AlMCM-41 [15] produce p-isomer. It is, however, noteworthy that the isomorphous substitution of Fe(III) in the silicate framework also leads to (moderate) acid catalysts, both in the microporous [16] and mesoporous [17] structures. Hence, they may be useful for the production of p-alkylated phenols. However, the mesoporous molecular sieves have certain advantages over their microporous counterparts, viz., high surface area, moderate acidity and mesoporosity. Keeping this in view, and in continuation of our earlier work [15], we have carried out the t-butylation of phenol over mesoporous H–FeMCM-41.

* To whom correspondence should be addressed.

2. Experimental

2.1. Synthesis and characterization

The FeMCM-41 sample with Si/Fe (molar) ratio of 50 was synthesized hydrothermally at 423 K for 9 days from a gel composition of $1SiO_2 : 0.5NaOH : 0.5CTAB : 0.01Fe_2O_3 : 0.108H_2SO_4 : 68H_2O$ [18]. The as-synthesized sample was calcined at 723 K for 8 h in air. All the samples were systematically characterized by powder X-ray diffraction (XRD, Rigaku), thermogravimetry/differential ther-

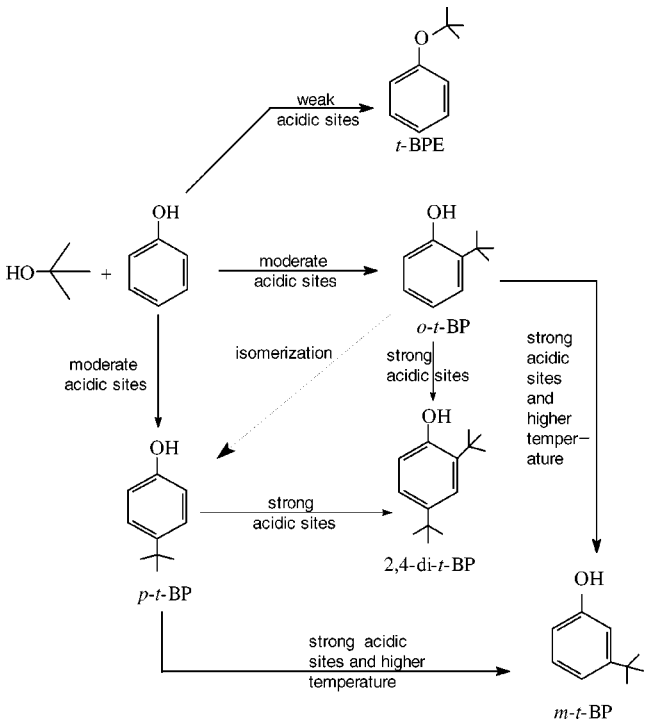

Figure 1. Effect of acid sites on the alkylation reaction of phenol with t-butyl alcohol.

mal analysis (TG/DTA, Dupont), BET surface area (Smartsorb 90), elemental analysis by inductively coupled plasma–atomic emission spectroscopy (ICP-AES, Plasmalab 8440), Fourier transform infrared (FT-IR, Nicolet), diffuse reflectance ultraviolet–visible (DRUV-vis, Shimadzu), and electron paramagnetic resonance (EPR, Varian) measurements. The acid form of the catalyst (H–FeMCM-41) was obtained by calcining the ammonium form of the catalyst (NH_4–FeMCM-41) at 773 K for 9 h in air. The latter was, however, prepared by repeated ion-exchange of the calcined FeMCM-41 with 1 M ammonium nitrate at 353 K for 6 h. The process was repeated thrice to obtain maximum exchange, and was then washed, filtered and dried at 373 K.

2.2. Temperature-programmed desorption of ammonia (TPDA)

The H–FeMCM-41 catalyst was subjected to ammonia adsorption followed by desorption as per the following procedure. About 200 mg of the sample was placed in a quartz reactor and activated at 773 K, initially in air for 6 h followed by helium for 2 h. The reactor was then cooled to 373 K and maintained for 1 h. Ammonia gas was then passed through the sample at this temperature for ∼15 min. Subsequently, helium was purged for 1 h to remove the physisorbed ammonia. Finally, the desorption of ammonia was carried out in a flow of helium with a heating rate of 10 K min^{-1}. The amount of ammonia desorbed from the catalyst was estimated with the aid of the thermal conducting detector response factor of ammonia.

2.3. Tertiary butylation of phenol

Alkylation of phenol with t-butyl alcohol was carried out in vapour phase using 750 mg of H–FeMCM-41 in a fixed-bed flow reactor with nitrogen as the carrier gas. Prior to the reaction, the catalyst was activated at 753 K in a flow air for 8 h. Then, it was cooled to the reaction temperature (448 K) under nitrogen. The reaction mixture, viz., phenol and t-butyl alcohol with desired (molar) ratio, was then fed into the preheated zone using a liquid injection pump (Sigma motor) with a space velocity of 4.8 h^{-1}. The gaseous products, viz., p-t-butylphenol (p-t-BP), o-t-butylphenol (o-t-BP) and 2,4-di-t-butylphenol (2,4-di-t-BP) were condensed and analyzed after every 30 min interval using gas chromatography (GC, Nucon 5700) with SE-30 column and 1% AT 1000 column. The products were further confirmed using a combined gas chromatography–mass spectrometer (GC-MS, Hewlett G1800A) with HP-5 capillary column.

3. Results and discussion

Both the as-synthesized and calcined samples were white in colour indicating the absence of bulk iron oxy-hydroxide and iron oxide impurity phases, respectively. TG of the as-synthesized sample showed a total weight loss of about 42%

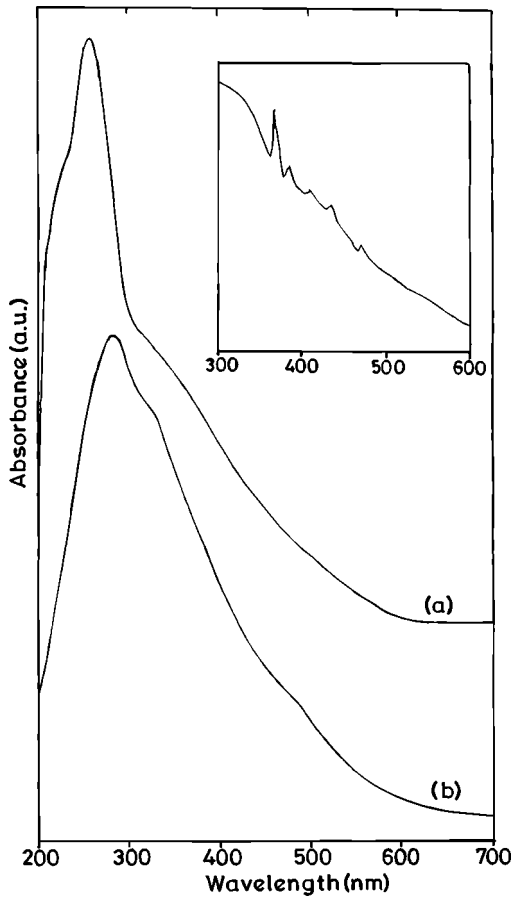

Figure 2. DRUV-vis spectra of FeMCM-41: (a) as-synthesized and (b) calcined.

(not reproduced here) indicating the mesoporous nature of FeMCM-41. The DTA results further support the observation [18]. XRD patterns of FeMCM-41 showed characteristic features of the hexagonal MCM-41 structure [19]. The main (100) reflection of FeMCM-41 was shifted towards the higher d value (d_{100} = 49.59 Å) compared to its siliceous analogue (d_{100} = 36.18 Å) [18]. That is, the substitution of Fe(III) for Si(IV) in the tetrahedral framework (crystal radii: Fe(III) = 0.63 Å; Si(IV) = 0.40 Å [20]) resulted in the expansion of the unit cell dimension. Further, a unique FT-IR absorption band at 660–670 cm^{-1}, assigned to Si–O–Fe symmetric stretching, supports the framework location of Fe(III). In addition, the appearance of two prominent absorption bands in DRUV-vis spectra (figure 2), i.e., a strong band at 250 nm associated with a shoulder at 215 nm accounts for the charge-transfer (CT) transitions involving Fe(III) in $(FeO_4)^-$ tetrahedral geometry [21]. This is further supported by the appearance of weak d–d transitions (see inset figure 2) between 300 and 500 nm [22]. However, upon calcination, the CT bands are shifted to higher wavelengths along with broadening of d–d bands, suggesting partial breaking of Si–O–Fe framework linkage [22].

The EPR spectra of the as-synthesized and calcined FeMCM-41 are shown in figure 3. As can be seen from this figure, there are three distinct signals ($g_{\text{eff}} \approx$ 4.3, 2.2 and 2.0) typical of three different Fe(III) environments [22–26].

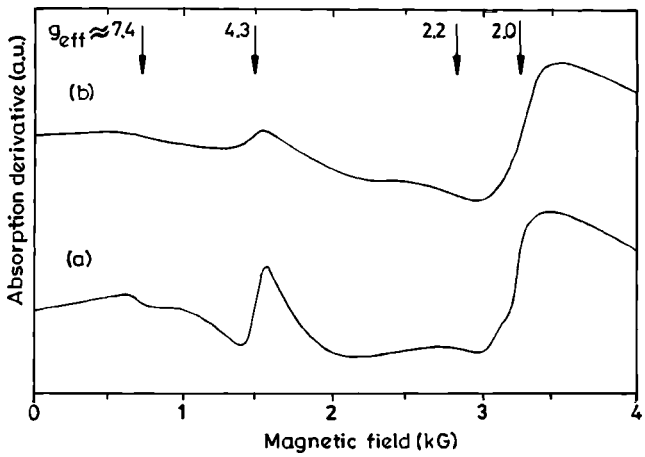

Figure 3. EPR spectra of FeMCM-41: (a) as-synthesized and (b) calcined.

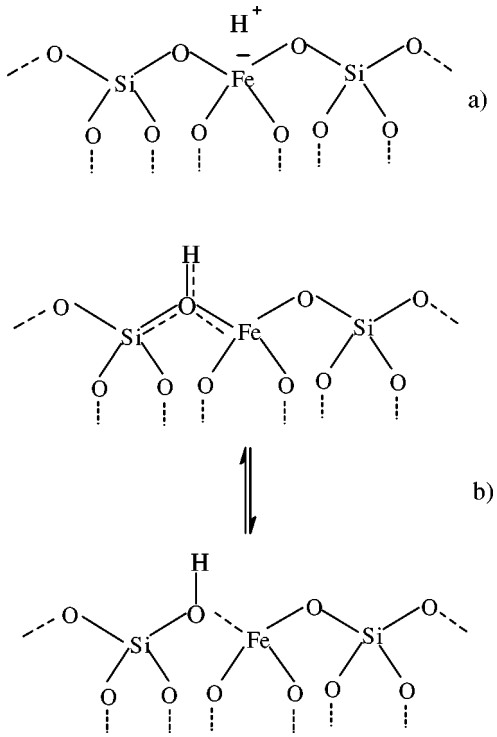

Figure 4. Schematic representation of different structural Fe(III) sites in FeMCM-41: (a) symmetrical site and (b) distorted site.

The intense higher field signal at $g_{\text{eff}} \approx 2.0$ is ascribed to Fe(III) in symmetrical (tetrahedral) environment (figure 4(a)), whereas the lower field signal at $g_{\text{eff}} \approx 4.3$ or above is assigned to trivalent iron in a distorted (tetrahedral) symmetry (figure 4(b)). On the other hand, the origin of the broad and weak band at $g_{\text{eff}} \approx 2.1$–$2.2$ is attributed to non-framework/superparamagnetic iron oxy-hydroxy/oxide clusters [28]. In the case of the calcined sample, the intensity of the lower field signal ($g_{\text{eff}} \approx 4.3$) is, however, reduced, thus suggesting a partial dislodgment of Fe(III) from the distorted framework sites. Further, the fraction of components corresponding to $g_{\text{eff}} = 4.3 : g_{\text{eff}} \approx 2.1$–$2.2$ is in the ratio of 6 : 29. This is in good agreement with the results of DRUV-vis studies as well as the low surface area of the FeMCM-41 (637 $m^2\,g^{-1}$), which falls in the range reported by Caravalho et al. [27]. However, the lower value could be attributed to the blocking of the internal (meso)pores by (non-framework) iron oxide nanoclusters [28]. Moreover, the lack of long-range ordering of the material along channels walls [29,30] may also contribute to the lowering of the value.

Figure 5 displays the TPDA profiles from H–FeMCM-41. The broad desorption pattern indicates a large distribution of different types of acid sites. Deconvolution of the profile results in three distinct peaks in the ranges 373–473, 408–508, and 443–608 K. They can be attributed to three different types of Brønsted acid sites which is, however, in good agreement with Kosslick et al. [31,32]. The three desorption peaks are described as follows: (i) the desorption peak at 473 K is assigned to weak acid sites due to surface/terminal hydroxyl groups; (ii) the peak at 465 K is attributed to moderate structural acid sites; and (iii) the peak at 524 K is assigned to strong structural acid sites. Finally, a broad desorption peak seen above 583 K is attributed to weak Lewis acid sites due to tricoordinated Fe(III) in the framework and/or Fe_xO_y particles generated upon calcination.

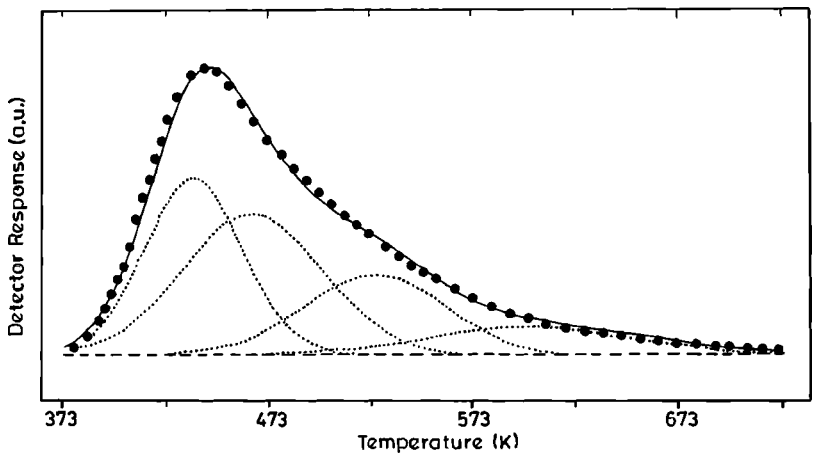

Figure 5. TPDA profiles of H–FeMCM-41.

Table 1
Tertiary butylation of phenol over H–FeMCM-41 catalyst with various phenol to t-butyl alcohol ratios at 448 K and WHSV = 4.8 h^{-1}.

	Phenol : t-butyl alcohol		
	2 : 1	1 : 2	1 : 4
Conversion (wt%)	8.4	21.1	21.0
Selectivity (%)			
p-t-BP	83.8	87.0	88.0
o-t-BP	16.2	9.5	8.7
m-t-BP	–	–	–
2,4-di-t-BP	–	3.5	3.3

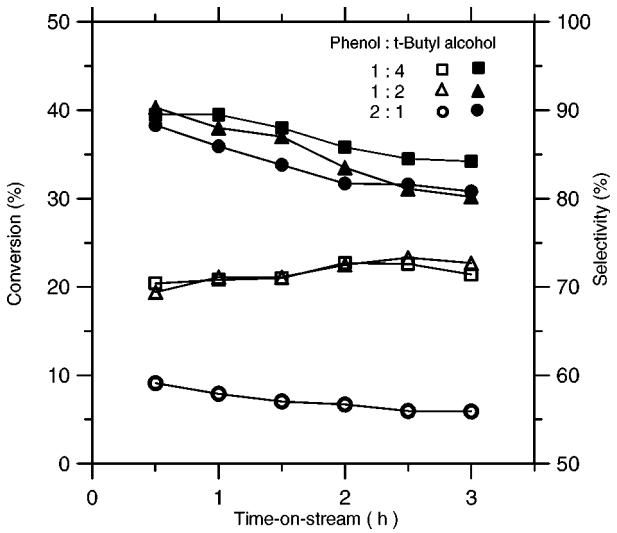

Figure 6. Phenol conversion and p-t-butylphenol selectivity over H–FeMCM-41: open symbols – conversion, filled symbols – selectivity.

The tertiary butylation reaction was carried out with different phenol : t-butyl alcohol ratios and the results are summarized in table 1. As stated earlier, a very good p-selectivity of the products is obtained compared to thermodynamically preferable m-isomer. This could be due to the fact that the hydroxyl groups of phenol favour o-/p-directing [7]. Moreover, the moderate acidic nature of H–FeMCM-41 is also responsible for the observed high p-selectivity. On the other hand, the m-isomer will form only with strong acid sites [7,11] through a 1,2 shift (secondary reaction, see figure 1). Although the conversion of phenol over H–FeMCM-41 is low as compared to its aluminium analogue [15] as well as with certain microporous materials [2,12], the selectivity of the p-t-butyl phenol is, however, on the higher side (see table 1). In fact, the lower conversion and the absence of m-alkylated product could be due to the relatively milder acidic characteristics of H–FeMCM-41 than H–AlMCM-41.

It is interesting to note that the increase in t-butyl alcohol amount in the reactants enhances the phenol conversion as well as p-selectivity of the product besides producing a small amount of 2,4-di-t-butyl phenol. Further, for a comparison, the catalytic activity of silica-supported iron oxide was also tested, which showed a very low (<1%) conversion. Figure 6 depicts the effect of time-on-stream on phenol conversion. As can be seen from this figure, no appreciable change in phenol conversion occurs but a slight decrease in selectivity was observed with increase in the reaction time. Further, the catalyst deactivates in <24 h time due to blocking of active sites by adsorbed molecules. However, upon activation (at 773 K for 6 h in air) the catalytic activity was restored.

4. Conclusion

From the above discussion, it was clearly demonstrated that trivalent iron is substituted isomorphously in the MCM-41 structure and that it exhibits symmetrical and distorted tetrahedral environments. The observed lower surface area could, however, be due to the blocking of mesopores by non-framework iron oxide which arise as a result of partial dislodgement of trivalent iron upon calcination. TPDA measurements show a moderate acid nature of H–FeMCM-41 and, hence, it shows a comparable conversion with good p-t-butylphenol selectivity to that of the analogous H–AlMCM-41 catalyst.

Acknowledgement

We thank Dr. P. Veluchamy for XRD and RSIC for EPR and GC-MS measurements.

References

[1] A. Knop and L.A. Pilato, *Phenolic Resins Chemistry* (Springer, Berlin, 1985).
[2] S. Subramanian, A. Mitra, C.V.V. Satyanarayana and D.K. Chakrabarty, Appl. Catal. A 159 (1997) 229.
[3] C.D. Chang and S.D. Hellring, US Patent 5 288 927 (1994).
[4] M. Yamamoto and A. Akyama, Jpn. Patent 6 122 639 (1994).
[5] A.U.B. Queiroz and L.T. Aikawa, French Patent 2 694 000 (1994).
[6] A. Corma, H. Garcia and J. Primo, J. Chem. Res. (1988) 40.
[7] R.F. Parton, J.M. Jacobs, D.R. Huybrechts and P.A. Jacobs, Stud. Surf. Sci. Catal. 46 (1988) 163.
[8] R.F. Parton, J.M. Jacobs, H.V. Ootehem and P.A. Jacobs, Stud. Surf. Sci. Catal. 46 (1988) 211.
[9] K. Zang, D. Xu, H. Zhang, S. Lu, C. Huang, H. Xiang and H. Li, Appl. Catal. A 166 (1998) 89.
[10] N.S. Chang, C.C. Chen, S.J. Chu, P.Y. Chen and T.K. Chuang, Stud. Surf. Sci. Catal. 46 (1988) 223.
[11] S. Namba, T. Yahima, Y. Itaba and N. Hara, Stud. Surf. Sci. Catal. 5 (1980) 105.
[12] A.J. Kolka, J.P. Napolitano and G.G. Elike, J. Org. Chem. 21 (1956) 712.
[13] B. Love and J.T. Massengale, J. Org. Chem. 22 (1957) 642.
[14] A. Mitra, Ph.D. thesis, I.I.T., Bombay (1997) p. 55.
[15] S.K. Badamali, A. Sakthivel and P. Selvam, in: *Proc. 2nd Pacific Basin Conf. Ads. Sci. Technol.*, eds. Do et al. (World Scientific, Singapore, 2000), in press.
[16] R. Szostak, *Molecular Sieves: Principles of Synthesis and Identification* (Van Nostrand Reinhold, New York, 1989).
[17] N. He, S. Bao and Q. Xu, Appl. Catal. A 169 (1998) 29.
[18] S.K. Badamali and P. Selvam, Stud. Surf. Sci. Catal. 113 (1998) 749.
[19] J.S. Beck, J.C. Vartuli, W.J. Roth, M.E. Leonowicz, C.T. Kresge, K.D. Schmitt, C.T.-W. Chu, D.H. Olson, E.W. Sheppard, S.B.

McCullen, J.B. Higgins and J.L. Schelnker, J. Am. Chem. Soc. 144 (1992) 10834.
[20] R.D. Shannon and C.T. Prewitt, Acta Crystallogr. B 25 (1969) 925.
[21] S. Bordiga, R. Buzzoni, F. Geobaldo, G. Lamberti, E. Giamello, A. Zecchina, G. Leofanti, G. Petrini, G. Tozzola and G. Vlaic, J. Catal. 158 (1996) 486.
[22] D.H. Lin, G. Coudurier and J.C. Védrine, in: *Zeolites: Facts, Figures, Future*, eds. P.A. Jacobs and R.A. van Santen (Elsevier, Amsterdam, 1989) p. 1431.
[23] T. Castner, G.S. Newell, W.C. Holton and C.P. Slichter, J. Chem. Phys. 32 (1960) 668.
[24] B.D. McNicol and G.T. Pott, J. Catal. 25 (1972) 223.
[25] D. Goldfarb, M. Bernardo, K.G. Strohmaier, D.E.W. Vaughan and H. Thomann, J. Am. Chem. Soc. 116 (1994) 6344.
[26] S.K. Badamali, R. Vinodhkumar, U. Sundararajan and P. Selvam, in: *Recent Trends in Catalysis*, eds. V. Murugesan, B. Arabindoo and M. Palanichamy (Narosa, New Delhi, 1999) p. 545.
[27] W.A. Caravalho, P.B. Varaldo, M. Wallau and U. Schuchardt, Zeolites 18 (1997) 408.
[28] P. Selvam, S.K. Badamali, M. Murugasen and H. Kuwano, in: *Recent Trends in Catalysis*, eds. V. Murugesan, B. Arabindoo and M. Palanichamy (Narosa, New Delhi, 1999) p. 556.
[29] F. Schuth, Ber. Bunsen Gen. Phys. Chem. 99 (1995) 1306.
[30] P. Behrens, Angew. Chem. Int. Ed. Engl. 35 (1996) 515.
[31] H. Kosslick, G. Lischke, B. Parlitz, W. Storek and R. Fricke, Appl. Catal. A 184 (1999) 49.
[32] H. Kosslick, H. Landmesser and R. Fricke, J. Chem. Soc. Faraday Trans. 93 (1997) 1849.